IOCCG Technical Series

Evaluation of Atmospheric Correction Algorithms over Turbid Waters

Editors: Cédric Jamet

Authors:

Sean Bailey, Xianqiang He, Cédric Jamet, Kevin Ruddick, Palanasimy Shanmugam, Thomas Schroeder, Knut Stamnes, Sindy Sterckx, François Steinmetz

International Ocean Colour Coordinating Group (IOCCG)

IOCCG, Darmouth, Canada

Décembre 2019

Evaluation of Atmospheric Correction Algorithms over Turbid Waters

IOCCG Technical Series Volume 1.0, 2019

Edited by:

Cédric Jamet

Report of an IOCCG Working Group chaired by Cédric Jamet with contributions from (in alphabetical order):

Sean Bailey, SAIC/NASA, USA

Chuqun Chen, South China Sea Institute of Oceanology, China

Xianqiang He, Satellite Ocean Environment Dynamics, Second Institute of Oceanography, China

Cédric Jamet, Laboratoire d'Océanologie et de Géosciences, Université du Littoral-Côte d'Opale, France

Kevin Ruddick, Remote Sensing and Ecosystem Modelling, Royal Belgian Institute of Natural Sciences, Belgium

Palanasimy Shanmugam, Indian Institute of Technology, India

Thomas Schroeder, CSIRO, Australia

Knut Stamnes, Stevens Institute of Technology, USA

François Steinmetz, Hygeos, France

Sindy Sterckx, VITO, Belgium

Correct citation for this volume:

IOCCG Technical Series (2019). Atmospheric Correction over turbid waters, Jamet, C. (eds.), Volume 1.0, IOCCG, Dartmouth, NS, Canada

This document is a product of an IOCCG working group

Table of contents

IOCCG Technical Series Report on Evaluation of atmospheric correction over turbid waters

IOCCG WG members:

Sean Bailey, SAIC/NASA, USA

Xianqiang He, SOED/SIO, China

Cédric Jamet, LOG/ULCO, France, chair

Kevin Ruddick, REMSEM/RBINS, Belgium

Palanasimy Shanmugam, ITT, India

Thomas Schroeder, CSIRO, Australia

Knut Stamnes, STI, USA

Sindy Sterckx, VITO, Belgium

Algorithm's providers: François Steinmetz for Polymer and Chuqun Chen for SWIRE

Sundarabalan

Introduction

This IOCCG Technical report is the result of an IOCCG on the evaluation of atmospheric correction algorithms over optically-complex waters that started in 2014. This report aims at being a complementary updated report of the IOCCG report # 10.

Optically-complex waters, especially turbid waters, have been the focus of several researches in the past decade and the IOCCG working group felt it was time to provide an exhaustive evaluation of the most common atmospheric correction used in the ocean color community but to provide guidances to the end-users on how and where to use a specific atmospheric correction algorithm.

As the reader may already know, the atmospheric correction process is vital to get accurate ocean color radiometry, i.e. the remote sensing reflectance (R_{rs}). While this process is somewhat easy in the open ocean waters (due to the fact that the ocean can be considered totally absorbent of the Sunlight), it is more complicated in optically-complex waters that are often observed in coastal waters.

Remote sensing of coastal waters is difficult as:

- these areas are highly variable in space and time
- the surrounding can affect the signal measured by the remote sensor (straylight contamination or adjacency effects)
- the aerosols are non-maritime (dust, pollution) and can be absorbing. These cases are not taking into account in most of atmospheric correction algorithms
- high values of high total suspended matter (SPM) and/or high colored dissolved organic matter concentrations (CDOM) can be observed. This complicates the estimation of R_{rs}(NIR) and the correction of the BRDF. Also, it can also saturate the remote sensor
- there are anthropogenic emissions (NO_2 absorption)

In this report, the WG decided to focus mainly on the turbid waters (non-zero R_{rs}(NIR)). This is mainly due to the availability of long-term time series of in-situ measurements in these coastal areas. The evaluation of the atmospheric correction algorithms has been done using MODIS-AQUA images. It does not mean that this report is focused on MODIS-AQUA, it's just an application. The main reason why MODIS-AQUA has been chosen is that it was the only remote sensor to have short-wave infra-red (SWIR) bands over a long-time period when the WG started. Since that, Sentinel-3A and Sentinel-3B as well as VIIRS have been launched. However, we believe that the results of this evaluation can be applicable to Sentinel-3 and VIIRS as the wavelengths are very similar and the principles of the algorithms in principle do not change with sensors (only the quality of the sensor changes). As the application of this report is on MODIS-AQUA, few atmospheric correction algorithms were not taking into account, especially the ones developed for MERIS sensor using the 709 nm band (Moore et al., 1999).

After presenting the different atmospheric correction algorithms included in the round-robin (Chapter 1), the three datasets used for the evaluation are presented in Chapter 2. Then the results over these three datasets including sensitivity studies (Chapter 3). The final chapter of this Technical Report presents the other issues that can occur when observing coastal waters (adjacency effects and absorbing aerosols) as well as results of other projects that evaluated atmospheric correction algorithms over optically-complex waters.

I. Atmospheric correction over turbid waters

This chapter presents the basis of the atmospheric correction and then the selected algorithms. The selection was based on availability of the algorithm and on the free will to share the code and to process the data. We tried to select algorithms that the community use or is interested in and algorithms that were based on different hypotheses so we could investigate the sensitivity of the outputs on those hypotheses.

1) Principles of the atmospheric correction

The purpose of the atmospheric correction process is to remove the contribution of the atmosphere to the signal measured by the remote sensor, leading to the estimation of the remote-sensing reflectance, i.e. the ocean color radiometry. The signal measured by the remote sensor at the top-of-the atmosphere can be decomposed into several terms (Gordon and Wang 1994; Gordon, 1997, IOCCG, 2010; Mobley et al., 2016; Frouin et al., 2019):

$$L_{TOA}=L_R+L_a+L_{ra}+T.L_g+t.L_{wc}+t.L_w \quad \text{(Eq. 1)}$$

with

- L_{TOA}, the radiance measured at the top of the atmosphere
- L_R, the radiance due to the air molecules (Rayleigh scattering)
- L_a, the radiance due to the aerosols (aerosols scattering)
- L_{ra}, the radiance due to the interaction between the aerosols and the air molecules (aerosols-Rayleigh scattering)
- L_g, the radiance due to the specular reflexion of the Sun on the sea surface (Sun glint
- L_{wc}, the radiance due to the white caps
- L_w, the water-leaving radiance (the final parameter)
- T, the direct transmittance
- t, the diffuse transmittance

The Rayleigh scattering, the white caps radiance and the Sun glint contributions as well as the gas absorption can be estimated from ancillary data (Mobley et al., 2016).

So the atmospheric correction process aims at estimating the contribution of the aerosols using the Rayleigh-corrected radiance:

$$L_{rc}=L_{TOA}- L_R= L_a+L_{ra}++t.L_w=L_A+t.L_w \quad \text{(Eq. 2)}$$

Over open ocean waters, the water-leaving radiance can be considered negligible (black pixel assumption) in the near-infrared (NIR) bands so the measured signal is only due to the aerosols. Using the NIR bands allow the estimation of the aerosol models and optical properties. But in more optically-complex waters, such as turbid waters (which are the main focus of the report), the black pixel assumption is not true anymore, as there is a contribution of the water to the top-of-atmosphere signal (IOCCG, 2010). To overcome this challenge, many atmospheric correction algorithms were developed in the past two decades for the major past and current ocean color remote sensors. They can be grouped into five different categories:

(1) assignment of the hypothesis on the NIR aerosols or water contributions (Hu et al., 2010; Ruddick et al., 2010), (2) use of the shortwave infrared bands [Wang and Shi, 2005; Wang and Shi, 2007; Wang, 2007; Shi and Wang, 2009, Chen et al., 2014, He and Chen, 2014], (3) use of blue or ultra-violet (UV) bands (Oo et al., 2008; He et al., 2012), (4) correction or modeling of the non/negligible ocean in the NIR (Moore et al., 1999; Siegel et al., 2000; Stumpf et al., 2003; Lavender et al., 2005; Bailey et al., 2010), and (5) coupled ocean/atmosphere inversion based on artificial neural networks (Doerffer and Schiller, 2007; Schroeder et al., 2007; Fan et al., 2017) or optimization techniques (Chomko et al., 2003; Stamnes et al., 2003; Jamet et al., 2004, Brajard et al., 2006, 2012; Kuchinke et al., 2009; Steinmetz et al., 2011).

The purpose is not to compare all existing atmospheric correction algorithms but to take the most used and the most different algorithms (i.e. based on different hypothesis and/or numerical methods).

2) Choice of algorithms

The algorithms used in the evaluation have been chosen on their availability and use by the ocean color community. The goal was not to have all published atmospheric correction algorithms but to have algorithms that are based on different hypothesis to try to understand how these hypothesis impact the accuracy of the retrievals.

a) NASA standard AC (Bailey et al., 2010)

The Bailey et al., (2010) approach estimates NIR reflectance through an iterative approach based on a reflectance retrieval in the red (670nm). The initial condition is based on the black-pixel assumption, from which an estimate of the visible reflectance is obtained. The backscatter coefficient in the red is estimated by inversion of the reflectance. This inversion assumes that the dominant absorption component is water, although an empirical estimate particulate absorption is employed as well. The backscatter slope parameter defined by Lee et al. (2010) is derived from the retrieved reflectance spectrum and is used to propagate the backscatter coefficient from the red into the NIR. This propagated backscatter coefficient is used in a forward model to retrieve an estimate of reflectance in the NIR which is subtracted from the signal prior to the next iteration of the atmospheric correction. The iteration is continued until convergence of the red reflectance or a maximum iteration threshold is reached.

b) NIR-SWIR AC (Wang and Shi, 2007)

This method combined the standard NASA atmospheric correction algorithm (Bailey et al., 2010) for the open ocean waters with an atmospheric correction method using the Short-Wave-Infra-Red (SWIR) bands (Wang and Shi, 2005). The switch is based on a turbidity index (Shi and Wang, 2007). The principle of the SWIR AC is the same as Gordon and Wang (1994), with considering the ocean being black in the SWIR bands. The epsilon parameter is calculated in the SWIR bands to then estimating the aerosol optical properties and models.

c) MUMM AC (Ruddick et al., 2000)

This algorithm replaces the assumption that the water leaving radiance is zero in the NIR by the assumptions of spatial homogeneity of the 748/869 nm ratios for aerosol and water-leaving reflectances over the subscene of interest. The ratio of ρ_A reflectances at 748 and 869 nm is named ε and is considered as a calibration parameter to be calculated for each sub-scene of interest. In addition, the ratio of ρw at 748 and 869 nm, named α, is also considered as a calibration parameter and is fixed to a value 1.945 for the MODIS-AQUA sensor (Ruddick et al., 2000, 2006). These assumptions are used to extend to turbid waters the GW94. Using the definition of α and ε, the equations defining $\rho_A(748)$ and $\rho_A(869)$ become:

$$\rho_A(748) = \varepsilon(748,869).\left[\frac{\alpha.\rho_{cor}(869)-\rho_{cor}(748)}{\alpha-\varepsilon(748,869)}\right] \quad (2)$$

$$\rho_A(869)\left[\frac{\alpha.\rho_{cor}(869)-\rho_{cor}(748)}{\alpha-\varepsilon(748,869)}\right] \quad (3)$$

The atmospheric correction algorithm can be summarized thus:

(1) Enter the atmospheric correction routine (i.e. GW94) to produce a scatter plot of Rayleigh-corrected reflectances $\rho_{cor}(765)$ and $\rho_{cor}(785)$ for the region of study. Select the calibration parameter ε on the basis of this scatter plot as described later.

(2) Reenter the atmospheric correction routine with data for Rayleigh-corrected reflectances $\rho_{cor}(748)$ and $\rho_{cor}(869)$ and use Eqs. (2) and (3) to determine $\rho_A(748)$ and $\rho_A(869)$, taking account of non-zero water-leaving reflectances.

(3) Continue as for the standard GW94 algorithm.

d) SWIRE AC (He and Chen, 2014)

A new shortwave infrared extrapolation (SWIRE) method is used to correct the NIR bands. The Rayleigh-corrected reflectances in the SWIR bands (1.24, 1.64, and 2.13 μm) are used to determine an exponential function with respect to wavelength, which is used to correct the NIR bands (0.748 and 0.869 μm) for sediment scattering and hence estimate the aerosol scattering reflectances in these bands. The Rayleigh-correction reflectances can be fitted with an exponential function in the NIR and SWIR bands for open ocean waters while only in SWIR for turbid waters. The fitted function is called the extrapolated Rayleigh-corrected reflectance and is used to calculate the epsilon parameter. Then the Gordon and Wang AC approach is applied.

e) NN-based AC (Fan et al., 2017)

Standard atmospheric correction (AC) algorithms work well in open ocean areas where the water inherent optical properties (IOPs) are correlated with pigmented particles. However, the IOPs of turbid coastal water may vary independently with pigmented particles, suspended inorganic particles, and colored dissolved organic matter (CDOM). In turbid coastal water, standard AC algorithms often exhibit large inaccuracies that may lead to negative water-leaving radiances (L_w) or remote sensing reflectances (R_{rs}). To address this problem new algorithms for retrieval of aerosol optical depth (AOD) and R_{rs} values, based on multilayer neural network (MLNN) methods, have been developed (Fan et al., 2017). A radiative transfer model for the coupled atmosphere-water system (AccuRT) is used to

simulate top of the atmosphere (TOA) radiances (L_{toa}) and R_{rs} values simultaneously, and this dataset is used to train MLNNs to determine AOD and R_{rs} values directly from L_{toa} radiances. The MLNN method has been validated using both synthetic data and Aerosol Robotic Network – Ocean Color (AERONET–OC) measurements. Application of these MLNN algorithms to MODIS Aqua images in several coastal areas shows that they are accurate (no negative R_{rs} values), robust, and resilient to contamination due to sunglint or adjacency effects of land and cloud edges. These MLNN algorithms are very fast once the neural networks have been properly trained and are therefore suitable for operational use. A significant advantage is that they do not need SWIR bands, which implies significant cost reduction for dedicated OC missions. These MLNN algorithms have been extended for application to extreme atmospheric conditions (i.e. strongly polluted continental aerosols) over turbid coastal water by including appropriate aerosol and ocean bio-optical models to generate the required training datasets. Application of these extended MLNN algorithms to VIIRS images over areas with extreme atmospheric and marine conditions (such as the Yellow Sea and the East China Sea) shows very promising results.

f) NN-based AC (Schroeder et al., 2007)

The ANN algorithm was adapted to an approach previously developed by Schroeder et al. (2007a, 2007b) [19, 35] for MERIS but on the basis of a different learning algorithm. In contrast to atmospheric correction algorithms based on the *Black-Pixel* assumption - the ANN method does not attempt to decouple atmospheric and oceanic light fields. Rather, it performs the correction directly on a pixel-by-pixel basis from the full TOA spectrum.

A scalar version of the Matrix-Operator-MOdel (MOMO) [36, 37] was used to simulate the light field in a coupled ocean-atmosphere system and to build a large data base of more than 20 million reflectance spectra at the bottom of the atmosphere (BOA) and at the top of the atmosphere (TOA). A variety of different sun and observing angles as well as different concentrations of oceanic and atmospheric constituents were considered in the simulations, which were subsequently used to adapt the ANN algorithm. The only difference in this study is the adaption of MODIS spectral band settings. ANN was implemented as a 3-layer perceptron and in this application represents a nonlinear function mapping between the TOA spectral reflectance (input) and the BOA spectral reflectance (output). Within such a network each layer consists of neurons – which are the basic, linear or non-linear, processing nodes. Each neuron is connected with each neuron of the next layer by a weight. The weights – in statistical term the free parameters - were estimated during a supervised learning procedure during which the network "learned" to associate an input vector $\vec{x}$ with a given output vector $\vec{y}$. The weights between two layers can be expressed as a matrix **W** and the complete analytic function represented by a 3-layer network is then given by the following equation:

$$\vec{y} = S_2 \times \{W_2 \times S_1(W_1 \times \vec{x})\}$$

In our case the activation function is linear for the output layer (S_2) and non-linear (logistic) for the hidden layer (S_1). Training of a network consisted of minimizing the sum of squared errors between all input and output training vectors by adapting the weight matrices ($\mathbf{W_1}$,$\mathbf{W_2}$) iteratively using a Limited Memory Broyden-Fletcher-Goldfarb-Shanno (L-BFGS) algorithm [38]. The training data was extracted randomly from the simulated data base. In detail, we extracted 100,000 spectra at BOA and TOA, of which one input vector $\vec{x}$ consisted of the full TOA spectral reflectance in MODIS ocean color bands 8-16 (λ=[412.5-869.5] nm), the angular information of the observing geometry transformed into Cartesian coordinates, the cosine of the sun zenith cos(θ_0) and the surface pressure *P*.

The associated output vector $\vec{y}$ contains the log-transformed remote sensing reflectance at BOA in the MODIS bands 8-15 (λ=[412.5-748] nm) and aerosol optical thickness (*AOT*) at four AERONET wavelengths (440, 550, 670 and 870 nm).

As there are no direct pathways to obtain the optimum network architecture, a series of 170 different networks were trained by varying the number of hidden layers, the number of neurons on the hidden layers and several noise levels. Training was stopped for each configuration after 1,000 iteration cycles over the full training data set of 100,000 spectra and monitored by the Mean Squared Error (MSE). The best performing network was selected based on the results obtained from match-up analysis – the ANN method therefore had the advantage in this AC comparison that it was tuned to the in-situ measurements. Its architecture consisted of 14 input nodes , 80 hidden layer neurons, and 12 neurons for the output layer trained with a random noise level of 0.8% for the TOA reflectance, 0.1% for each the geometry inputs and 2% for the surface pressure.

g) Polymer AC (Steinmetz et al., 2011)

The Polymer atmospheric correction algorithm (Steinmetz et al, 2011, Steinmetz et al, 2018) is an advanced full-spectrum coupled spectral matching algorithm for Ocean Colour. It was originally developed for the atmospheric correction of MERIS observations, in particular in presence of sun glint contamination, but has been extended to many other sensors. This algorithm relies firstly on a water reflectance model based on (Park & Ruddick, 2005) having only two unknown parameters, the chlorophyll concentration and the particle backscattering, to represent a large variability of the oceanic and coastal waters. Secondly, it relies on a model for the atmosphere and surface reflectance, whose particularity is to be represented as a linear combination of three terms: $\rho_{ag}(\lambda) = T_0(\lambda)c_0 + c_1\lambda^{-1} + c_2\rho_{mol}(\lambda)$. This analytical formulation does not rely on aerosol models and allows fitting accurately not only the aerosol reflectance, but also other complex atmospheric and surface effects, in particular the residual sun glint. This formulation essentially relies on the general fact that atmospheric effects in $\rho_{ag}(\lambda)$ are spectrally smooth.

An iterative optimization scheme is applied pixel by pixel, using the Nelder-Mead simplex method, to retrieve the water and atmospheric parameters simultaneously. The final values of $\rho_{ag}(\lambda)$ are subtracted from the observation, so that the final water reflectance is not the output of the model, and preserves fine spectral features from the observation.

Polymer is freely available for non-commercial purposes on www.hygeos.com/polymer.

h) Gaussian-spectral relationships SS14 (Singh and Shanmugam, 2014)

Estimation of aerosol radiance remains a challenging problem in the process of atmospheric correction of ocean color data due to its random variability in space, time, and type that increase the complexity of its estimation with the conventional methods. The higher radiance values in the near infrared (NIR) region due to turbidity interferes with the standard aerosol correction which generally performs well in open ocean waters. To improve the performance of aerosol correction method, the radiance values must be corrected for contributions by the water constituents. To mitigate this problem, a correction factor, *κ*, is introduced which is defined in terms of band ratio to determine the extent of radiance contributed by various optically active water constituents in the NIR bands (Singh and Shanmugam, 2014). The band ratio of *κ* is determined differently for each water type, such as green to blue band

for sediment dominated waters, fluorescence to absorption red band for in-water blooms, shorter NIR to red band for dense algal blooms, whereas κ is unity for clear water where no correction in NIR band is required. Once, the NIR band has been corrected for the elevated signal in the optically complex water signals, the radiance values can be extrapolated to visible bands for better estimation of aerosol radiance. To achieve this, Rayleigh corrected NIR band radiance and κ are employed to determine reference radiance (L_{ref}) in the green region, wherein the magnitude of aerosol radiance remains maximum, and hence the relative error in estimation of L_{ref} reduces to a minimum level. Due to the empirical relationship between the corrected NIR band and L_{ref}, there lies a probability of over-estimation. The elevated signal in the NIR band is generally attributed to the scattering by phytoplankton, which also tends to absorb in the red region. Such absorption feature in the red region can be utilized to reiterate the estimation of L_{ref} and minimize the over-estimation. Using L_{ref}, aerosol radiance ($L_a(\lambda)$) can be estimated using a Gaussian extrapolation over the entire visible spectrum. However, such extrapolation fails to determine the aerosol radiance for the longer NIR band, and hence, the aerosol radiance is assumed to be smooth in this region and extended to the longer NIR band. The major benefit of the method can be attributed to the need of only standard ocean color bands to determine κ, which makes it widely applicable to most of the ocean color sensors.

i) UV-based AC (He et al., 2012)

The principle of the UV-AC algorithm is based on the fact that the water-leaving radiance at ultraviolet wavelengths can be neglected as compared with that at the visible light wavelengths or even near-infrared wavelengths in most cases of highly turbid waters due to the strong absorption by detritus and colored dissolved organic matter [1]. In turbid waters, the water-leaving radiances increase largely at longer VIS wavelengths and NIR due to strong particulate scattering, yet the strong combined absorption by detritus and CDOM contents cause a rapid decrease of the water-leaving radiance at the UV band [2]. In extremely turbid waters, such as the Hangzhou Bay, the water-leaving radiance at the UV band is much lower than at the NIR band. In such turbid coastal and inland waters, the UV band is more suited than the NIR band for estimating the aerosol scattering radiance [3]. Since most of the launched satellite ocean color sensors have no UV band, the shortest wavelength (usually at 412nm) can be used. Taking the SeaWiFS for an example, the shortest waveband (412 nm) was used as the reference to estimate the aerosol scattering radiance. Assuming that the water-leaving reflectance at 412 nm can be neglected in highly turbid waters, we can estimate the aerosol scattering reflectance at 412nm [$\rho_a(412nm) = \rho_{rc}(412nm)$]. Based on the extrapolation method with fairly accurate method, we can estimate the aerosol scattering reflectance at 865 nm.

$$\begin{cases} \rho_a(865nm) = \rho_{rc}(412nm)\exp\left[c(412-865)\right] \\ c = \ln\left[\rho_{rc}(765nm) / \rho_{rc}(865nm)\right] / (865-765) \end{cases}$$

For the reality applications, the UV-AC algorithm was applied to the whole target region which might not only cover the turbid waters, but also include some of the clear waters. To avoid the overestimation of the aerosol scattering reflectance in clear waters, the $\rho_a(865nm)$ is limited to $\rho_{rc}(865nm)$. Specifically, when the estimated $\rho_a(865nm)$ is larger than the $\rho_{rc}(865nm)$, it will be set as $\rho_{rc}(865nm)$. Finally, a "white" aerosol scattering reflectance spectrum is assumed to the whole target region, and the aerosol scattering reflectance at all bands will be equal to $\rho_a(865nm)$.

II. Dataset

a) Simulated dataset

An enhanced version of the simulated dataset developed in the IOCCG report #10 has been developed to encompass a wide range of coastal waters.

The AccuRT radiative transfer code has been used to generate the radiances at the top-of-the-atmosphere, at the top-of-the-atmosphere corrected from the gas absorptions, at the top-of-the-atmosphere corrected from the gas absorptions and the Rayleigh scattering, the aerosol and Rayleigh/aerosol radiance, the diffuse transmittance and the remote-sensing reflectance (Jin and Stamnes, 1994; Thomas and Stamnes, 1999; Cohen et al., 2013; Hamre et al., 2014).

The aerosol model are from Ahmad et al. (2010) and the inherent optical properties of the seawater from the COASTCOLOUR project ()

In order to cover a wide range of atmospheric and water conditions, we generated 20,000 cases as follows:

For each ocean case, 4 aerosol models were randomly selected among the 80 possible models (4 aerosol configurations x 5,000 water configurations). For each of these 20,000 cases, the geometry angles were randomly selected in the following ranges:

- Solar zenith angle (θ_s = SZA): 0-70°

- Viewing zenith angle (θ_v = VZA): 0-70°

- Relative azimuth angle ($\Delta\Phi = \Phi_s - \Phi_v$ = RAA): 0-180°.

The sun-glint geometry were avoided in the simulations.

The simulated dataset has been generated for SeaWiFS, MODIS-AQUA, VIIRS, MERIS and OLCI sensors. The following files are therefore provided with the dataset:

1. "sensor_InputParameter.txt",

2. "sensor_RadianceTOA.txt",

3. "sensor_RadianceTOA gas corrected.txt",

4. "sensor_RadianceTOA gas&rayleigh corrected.txt"

5. "sensor_Rrs.txt"

6. "sensor_aerosolReectance.txt"

7. "sensor_diffuseTransmittance.txt"

The file "sensor_InputParameter.txt" contains the input parameters for the simulations. The format is as follows: SZA, VZA, RAA, $\tau_a(865)$, angstrom(443/865), f_v, RH, CHL, CDOM, MIN.

The file "sensor_RadianceTOA.txt" includes the top of atmosphere (TOA) radiances for each simulation case. These radiances were simulated with atmospheric gas absorption, Rayleigh scattering, aerosol and ocean IOPs turned on. The number of columns in the file depends on the sensor. For example, there are 16 columns in each line for MODIS, one for each band.

The file "sensor_RadianceTOA_gas_corrected.txt" contains "atmospheric-gas-corrected" TOA radiances for each simulation case. The radiances were simulated with atmospheric gas absorption turned off, but Rayleigh scattering, aerosol, and ocean IOPs turned on. The number of columns in the file depends on the sensor. For example, there are 16 columns in each line for MODIS, one for each band. These radiances can be used to validate the atmospheric gas correction algorithm.

The file "sensor_RadianceTOA_gas&rayleigh_corrected.txt" contains "atmospheric-gas-and- Rayleigh-corrected" TOA radiances using data from "sensor_RadianceTOA_gas_corrected.txt" with the pure Rayleigh scattering radiances subtracted. The pure Rayleigh scattering radiances were simulated with only Rayleigh scattering turned on, and atmospheric gas absorption, aerosol, and ocean IOPs turned off. The number of columns in the file depends on the sensor. For example, there are 16 columns in each line for MODIS, one for each band.

The file "sensor_Rrs.txt" contains the remote sensing reflectance Rrs for each simulation case. The remote sensing reflectance was computed as the water leaving radiance divided by the downwelling irradiance just above the surface. The water leaving radiance was simulated as described in Appendix C. The simulation was done with atmospheric gas absorption, Rayleigh scattering, and aerosols turned on in the atmosphere. This file includes two sets of data. The first half of the columns include nadir Rrs values (θ_0= SZA; θ= 0; $\Delta\Phi$ = 0) and the second half of the columns include the corresponding Rrs values at the geometry of (θ_0= SZA; θ = VZA; $\Delta\Phi$ = RAA). For example, there are 32 columns in the file "MODIS Rrs.txt". The first 16 columns contain the nadir Rrs values (SZA, 0, 0) for each band, while the next 16 columns contain the corresponding Rrs values at geometry (SZA, VZA, RAA). The second set of Rrs data can be used to validate the atmospheric correction algorithm. The first set of Rrs data can be used to validate the BRDF algorithm.

The file "sensor_aerosolReflectance.txt" contains the reflectance for aerosols (no molecular scattering or absorption, but including molecule/aerosol interactions) at the TOA. These reflectances were computed as $Radiance_{aerosol}(TOA)/E_d(TOA)$, and correspond to $\rho_a + \rho_{ra}$ as defined by Gordon and Wang (1994). **But please note that there is a factor of π difference: Gordon and Wang (1994) defines the reflectance as $\rho = \pi L/(\mu_0 F_0)$, while we use $\rho = L/(\mu_0 F_0)$.**

The file "sensor_diffuseTransmittance.txt" contains two-way diffuse transmittance for aerosols and molecular scattering (no molecular absorption).

b) In-situ dataset

An in-situ dataset of remote-sensing reflectance and aerosol optical thickness have been gathered. These measurements are from the AERONET-Ocean Color network (Zibordi et al., 2009b). AERONET-OC is the ocean component of the Aerosol Robotic Network (AERONET, Holben et al., 1998). AERONET-OC is a system of autonomous sun photometers distributed around the globe (mainly in the northern hemisphere as shown in Figure XX) providing normalized water-leaving (nL_w) radiance and the aerosol optical thickness at multi-wavelengths in the visible.

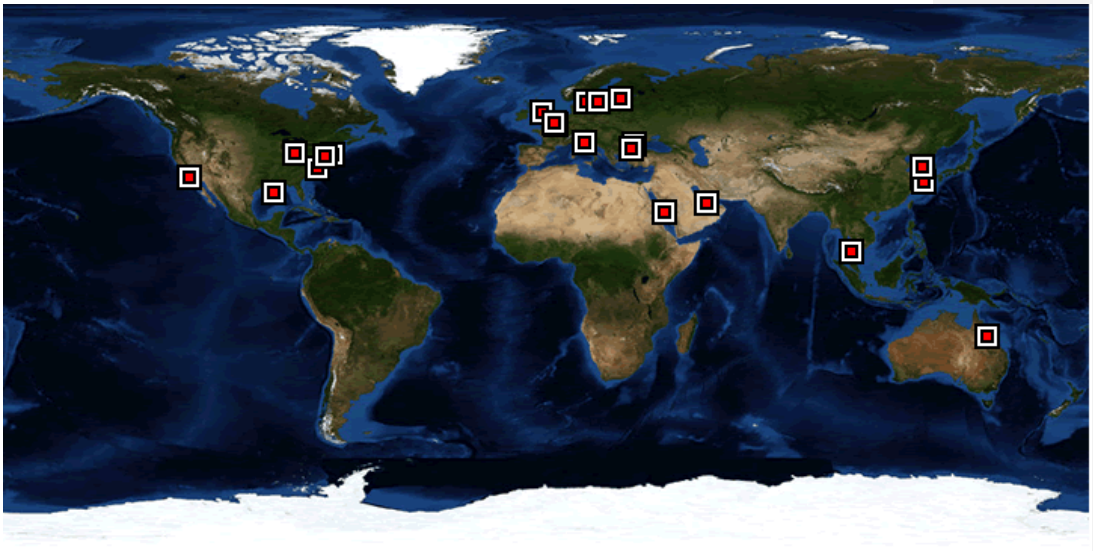

Figure : Maps of the global AERONET-OC stations. The stations used in this report are mentioned in table 1

The advantage of using AERONET-OC data is that the production of the measurements is standardized with identical systems and protocols, with calibration from a single source or method and with processing using the same code (Zibordi et al., 2006; 2009). Moreover, measurements are taken several times a day, every day (optimally), which leads to a high number of potential match-ups.

Table 1 presents the different AERONET-OC stations used for the match-ups exercise.

Table 1. AERONET-OC stations names, locations and number of data used

S.No	Station	Year	Lat	Lon	N	Nv
1	VENISE	2002-2015	45.31	12.50	1192	
2	COVE	2006-2015	36.90	-75.71	38	
3	GDLT	2005-2015	58.59	17.46	268	
4	HLT	2006-2015	59.94	24.92	261	
5	MVCO	2004-2015	41.30	-70.55	412	
6	GLORIA	2011-2015	44.59	29.35	186	
7	LUCINDA	2009-2015	-18.50	146.30	83	
8	ZEEBRUGGE	2014	51.36	3.12	16	

Characteristics of the selected AERONET-OC stations are provided in Feng et al. (2008); Zibordi et al. (2009a); Zibordi et al. (2015); Van der Zande (2016).

c) Images dataset

It is useful to directly look at the images to observe the behaviors of the atmospheric correction algorithms.

III. Match-ups analysis

1) Extraction of the match-ups

The validation of the algorithms have been done through a classic match-ups analysis (Bailey et al., 2006). The following steps have been taken:

1. 1-hour interval between the satellite overpass and the AERONET-OC measurement
2. Extraction over a 3-by-3-pixel box centered over the AERONET-OC station
3. 6 out of 9 pixels must be valid over the 3-by-3-pixel box
4. A coefficient of variability, CV, is calculated, i.e. standard deviation/mean values over the 3-by-3-pixel box
5. A match-ups is valid if CV<0.2
6. Calculation of the mean values over the valid pixels
7. AERONET-OC data are filtered for taking into account only turbid waters as defined by Robinson et al. (2003): Rrs(667)>0.0012

Considering these different steps, out of 2456 possible match-ups, only 889 remained.

2) Statistical parameters

To quantitatively evaluate the performances of the algorithms the following statistical parameters have been calculated:

- Relative Error: $RE = \frac{1}{N}\sum\left(100 \times \frac{|R_{rs}^{sat} - R_{rs}^{obs}|}{R_{rs}^{obs}}\right)$
- Root-Mean-Square-Error: $RMSE = \sqrt{\left(\frac{\sum\left(R_{rs}^{sat} - R_{rs}^{obs}\right)^2}{N}\right)}$
- Slope and intercept of the regression line
- Bias: $BIAS = \frac{1}{N}\sum\left(100 \times \frac{R_{rs}^{sat} - R_{rs}^{obs}}{R_{rs}^{obs}}\right)$
- Correlation coefficient R^2

3) Statistical evaluation of the retrieved spectra

Aside the classic statistical parameters, investigations on the shape of the retrieved spectra were also performed through three parameters:

- Quality Assurance Score (QAS; Wei et al., 2016): this parameter provides quantification of the full R_{rs} spectrum quality of retrievals with regards to reference spectra. The value has to be 1.
- χ^2: this parameter provides information about the full spectrum relative errors. The value has to be 0.
- the Spectral Angle Mapper (SAM; Kruse et al., 1993; Keshava, 2004): this parameter indicates the mean of the full spectrum difference between the retrieved R_{rs} and in-situ R_{rs} spectra. The values has to be 0°.

d) Ranking of the algorithms using a score scheme

The scoring scheme developed by Müller et al. (2015) have been used to classify the algorithms. It is based on the values of the slope and intercept of the linear regression, BIAS, RMSE, RE and R^2 and the number of valid match-ups. The highest possible score is the number of parameters times the number of wavelengths. In our case, the maximal value is 42. This scheme converts the statistical parameters into relative scores.

IV. Results

1) Simulated dataset

2) In-situ dataset

REMAKE THE SCATTERPLOTS BY REMOVING THE OLD ALGORITHM FROM STAMNES

a) Global match-up analysis

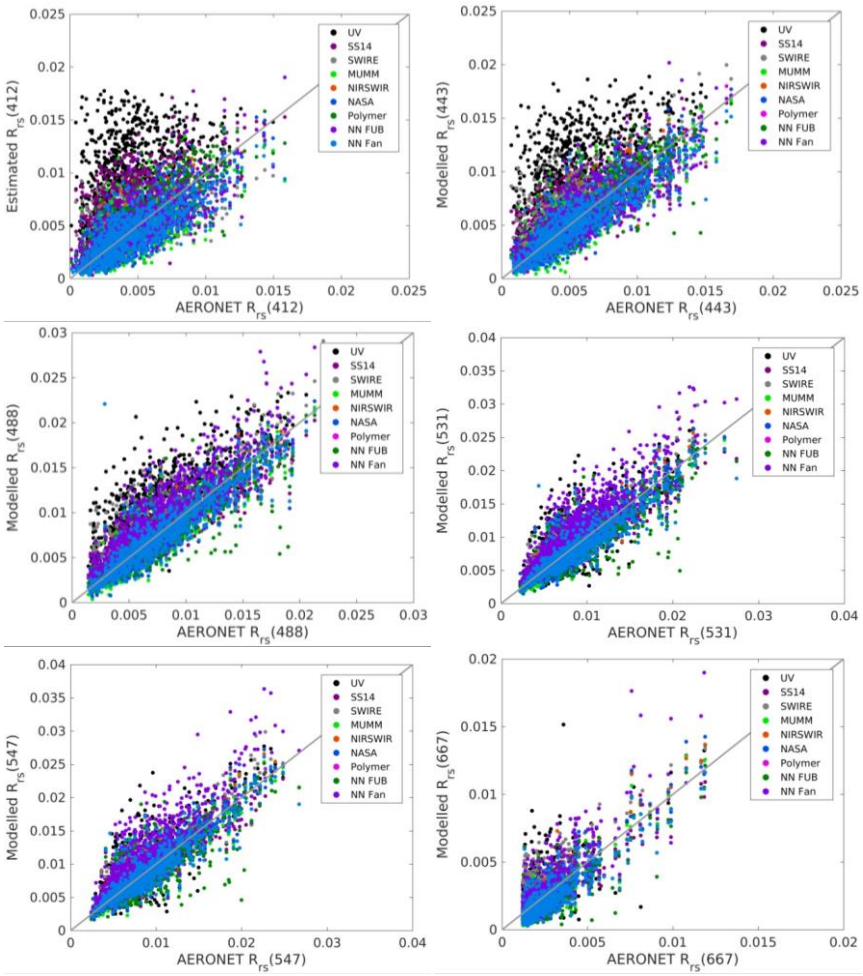

Figure XX: Scatterplots of the AC estimated R_{rs} vs in-situ R_{rs} from 412 (top left) to 667 nm (bottom right).

Table 1: The statistical results derived from the remote sensing reflectance, R_{rs} derived from various atmospheric correction algorithms and AERONET data R_{rs} (*RE* - mean relative error, *RMSE* – root mean square error, R^2-regression, *Nvm*- number of valid data/model/wavelength, *CV* = coefficient of variation, N = number of input data)

	RE(%)	*RMSE*	Slope	Intercept	Bias	R^2	*Nvm*	R_{rs}<0	*CV<0.2*
NASA STD AC Model									
R_{rs} *(412)*	38	0.00168	1.02	0.000261	0.000334	0.63	703	6	180
R_{rs} *(443)*	26	0.00144	0.98	0.00035	0.000225	0.81	775	0	114
R_{rs} *(488)*	19	0.00155	0.98	0.000498	0.000359	0.87	819	0	70
R_{rs} *(531)*	16	0.00169	0.96	0.000732	0.00038	0.86	803	0	86
R_{rs} *(547)*	15	0.00165	0.94	0.000831	0.000283	0.85	788	0	101
R_{rs} *(667)*	39	0.00074	0.85	0.000601	0.000269	0.86	582	0	307
NIR-SWIR AC Model									
R_{rs} *(412)*	35	0.00174	1.01	0.00018	0.000233	0.62	613	3	273
R_{rs} *(443)*	23	0.00148	0.97	0.00026	0.000106	0.80	677	0	212
R_{rs} *(488)*	17	0.00157	0.98	0.000387	0.00023	0.86	725	0	164
R_{rs} *(531)*	15	0.00174	0.96	0.000648	0.000282	0.84	750	0	139
R_{rs} *(547)*	15	0.00168	0.94	0.000758	0.000197	0.85	754	0	135
R_{rs} *(667)*	38	0.00079	0.83	0.00058	0.000189	0.86	488	0	401
MUMM AC Model									
R_{rs} *(412)*	46	0.00203	1.06	0.000155	0.000448	0.49	552	19	318
R_{rs} *(443)*	34	0.00169	1.01	0.000325	0.00039	0.73	665	5	219
R_{rs} *(488)*	24	0.00168	1.00	0.000482	0.000507	0.85	720	0	169
R_{rs} *(531)*	18	0.00178	0.99	0.000621	0.000512	0.84	726	0	163
R_{rs} *(547)*	17	0.00173	0.96	0.000713	0.000395	0.84	714	0	175
R_{rs} *(667)*	54	0.00083	0.89	0.000624	0.000411	0.82	529	0	360
SS14 AC Model									
R_{rs} *(412)*	39	0.00323	0.98	-0.00211	-0.00228	0.40	889	0	0
R_{rs} *(443)*	28	0.00227	1.15	-0.00231	-0.00124	0.64	889	0	0
R_{rs} *(488)*	20	0.00184	1.24	-0.00233	-0.0004	0.81	889	0	0
R_{rs} *(531)*	17	0.00189	1.20	-0.00206	-0.00024	0.80	889	0	0
R_{rs} *(547)*	16	0.00180	1.15	-0.00166	-0.00028	0.80	889	0	0
R_{rs} *(667)*	27	0.00071	1.04	2.68E-05	0.000116	0.76	889	0	0
SWIRE AC model									
R_{rs} *(412)*	45	0.00274	1.30	-0.00163	-7.3E-05	0.15	264	0	625
R_{rs} *(443)*	29	0.00275	1.15	-0.0025	-0.00134	0.51	499	0	390
R_{rs} *(488)*	23	0.00291	1.05	-0.00227	-0.00181	0.73	508	0	381
R_{rs} *(531)*	18	0.00253	1.00	-0.00111	-0.00114	0.76	495	0	394
R_{rs} *(547)*	18	0.00251	0.94	-0.0006	-0.00121	0.77	481	0	408
R_{rs} *(667)*	30	0.00139	0.84	-0.00035	-0.00086	0.70	393	0	496

	RE (%)	*RMSE*	Slope	Intercept	Bias	R^2	*Nvm*	R_{rs}<0	*CV<0.2*
UV AC Model									
R_{rs} *(412)*	53	0.00629	0.69	-0.00219	-0.00523	0.14	793	0	96
R_{rs} *(443)*	45	0.00537	0.82	-0.00266	-0.00445	0.35	812	0	77
R_{rs} *(488)*	33	0.00423	0.91	-0.00237	-0.00329	0.61	819	0	70
R_{rs} *(531)*	23	0.00301	0.93	-0.0006	-0.0013	0.62	782	0	107
R_{rs} *(547)*	23	0.00299	0.88	-5.4E-05	-0.00124	0.61	770	0	119
R_{rs} *(667)*	35	0.00144	0.75	0.00013	-0.00057	0.47	670	0	219
Polymer AC Model									
R_{rs} *(412)*	21	0.00144	1.00	-0.00051	-0.00048	0.76	886	2	0
R_{rs} *(443)*	19	0.00143	1.09	-0.00068	-0.00014	0.80	886	2	0
R_{rs} *(488)*	17	0.00182	1.13	-0.00078	0.000196	0.80	886	2	0
R_{rs} *(531)*	19	0.00220	1.11	-0.0004	0.000561	0.74	886	2	0
R_{rs} *(547)*	18	0.00216	1.05	-0.00016	0.00028	0.72	886	2	0
R_{rs} *(667)*	44	0.00087	1.00	0.000331	0.000334	0.71	886	2	0
NN FUB AC model									
R_{rs} *(412)*	27	0.00165	1.05	-0.00031	-8.2E-05	0.63	889		
R_{rs} *(443)*	24	0.00173	1.08	-0.00046	-2.4E-05	0.71	889		
R_{rs} *(488)*	23	0.00273	0.91	-0.00089	-0.00177	0.78	889		
R_{rs} *(531)*	22	0.00330	0.83	-0.00053	-0.00243	0.80	889		
R_{rs} *(547)*	21	0.00342	0.79	4.09E-05	-0.00234	0.77	889		
R_{rs} *(667)*	27	0.00116	0.69	0.000555	-0.00026	0.73	889		
NN Fan AC model									
R_{rs} *(412)*	35	0.00208	1.01	0.000224	0.000268	0.47	888		
R_{rs} *(443)*	23	0.00165	1.09	-0.00023	0.000278	0.74	888		
R_{rs} *(488)*	15	0.00162	1.07	-0.00026	0.00029	0.85	888		
R_{rs} *(531)*	15	0.00179	1.08	-0.00013	0.000561	0.83	888		
R_{rs} *(547)*	13	0.00170	1.01	0.000151	0.000239	0.83	888		
R_{rs} *(667)*	43	0.00079	1.00	0.000415	0.000418	0.79	888		

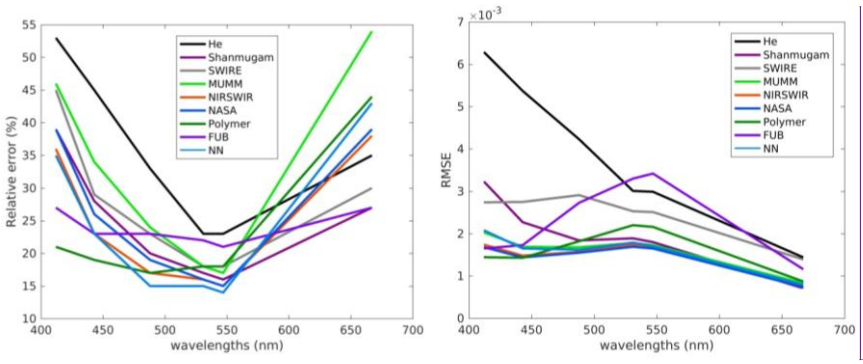

Figure : (a) Variation of the relative error as a function of the wavelength, (b) Variation of the RMSE as a function of the wavelength

Commented [j1]: AVOIR LE MEME NOM DES ALGOS ENTRE LE TEXTE, LES TABALEAUX ET LES FIGURES

ANALYSIS OF THE RESULTS

- NUMBER OF MATCHUPS

- SCATTERPLOTS

- VARIATION OF STATISTICAL PARAMETERS

- VARIATION OF SPECTRA PARAMETERS

b) Common match-ups analysis

c) Sensitivity studies

On the global match-ups

Variation of the statistical parameters as a function of environmental parameters have been studied.

- Turbidity (Nechad et al., 2012)
- Aerosol optical thickness (from AERONET-OC)
- SPM (Han et al., 2016)

3) Images dataset

V. Other issues

1) adjacency effects (Sindy Sterckx)

2) Absorbing aerosols (Cédric Jamet)

Most of the atmospheric correction algorithms do not take into account absorbing aerosols (dust, pollution). It is especially true for the standard AC from the space agencies. The reason is that it is complicated to handle and all the already published method are time-consuming. Absorbing aerosols, especially dust, are not detectable using only NIR bands as they have a spectral dependency.

The AC incorporating absorbing aerosols have been mostly developed for open ocean waters (Moulin et al., 2001a, 2001b; Chomko and Gordon, 1998, Chomko et al., 2001; Banzon et al., 2009; Nobileau and Antoine, 2005) and were specifically designed to only detect absorbing aerosols. Few tackle in the same time non-zero R_{rs}(NIR) and absorbing aerosols. Most of them us spectral optimization algorithms to estimate R_{rs} (Brajard et al., 2006, 2012; Kuchinke et al., 2009).

3) C2X and EUMETSAT Mazeran (Voir avec Carsten et Constant)

VI. Conclusion

References

Ahmad, Z., B. A. Franz, C. R. McClain, E. J. Kwiatkowska, J. Werdell, E. P. Shettle, and B. N. Holben, New aerosol models for the retrieval of aerosol optical thickness and normalized water-leaving radiances from the SeaWiFS and MODIS sensors over coastal regions and open oceans, Appl Opt. 49, 5545-5560, 2010.

Banzon, V.F., H.R., Gordon, C.P., Kuchinke, D., Antoine, K.J., Voss and R.H., Evans (2009). Validation of a SeaWiFS dust-correction methodology in the Mediterranean Sea: Identification of an algorithm-switching criterion, Remote Sensing of Environment, 113, 2689-2700.

Brajard, J., C., Jamet, C., Moulin and S., Thiria (2006). Use of a neurovariational inversion for retrieving oceanic and atmospheric constituents from ocean color imagery: Application to absorbing aerosols, Neural Networks, 19, 178-185.

Brajard, J., R., Santer, M., Crépon and S., Thiria (2012). Atmospheric correction of MERIS data for case-2 waters using a neuro-variational inversion, Remote Sensing of Environment, 126, 51-61.

Chomko, R.M., and H.R., Gordon (2001). Atmospheric correction of ocean color imagery: test of the spectral optimization algorithm with the Sea-viewing Wide Field-of-view Sensor, Applied Optics, 40, 2973-2984.

Chomko, R.M., and H.R., Gordon (1998). Atmospheric correction of ocean color imagery: use of the Junge power-law aerosol size distribution with variable refractive index to handle aerosol absorption, Applied Optics, 37, 5560-5572.

Chomko, R.M., H.R., Gordon, S., Maritorena and D.A., Siegel (2003). Simultaneous retrieval of oceanic and atmospheric parameters for ocean color imagery by spectral optimization: a validation, Remote Sensing of Environment, 84, 208-220.

Cohen, D., S. Stamnes, T. Tanikawa, E. R. Sommersten, J. J. Stamnes, J. K. Lotsberg, and K. Stamnes, Comparison of discrete ordinate and Monte Carlo simulations of polarized radiative transfer in two coupled slabs with different refractive indices, Opt. Expr., 21, 9592-9614, 2013. DOI:10.1364/OE.21.009592.

Doerffer, R., and H., Schiller (2007) The MERIS case 2 water algorithm, International Journal of Remote Sensing, 28, 517-535.

Dogliotti, A. I., K.G., Ruddick, B., Nechad, D., Doxaran, and E., Knaeps (2015). A single algorithm to retrieve turbidity from remotely- sensed data in all coastal and estuarine waters, Remote Sensing of Environment, 156, 157-168.

Fan, Y., W. Li, C. K. Gatebe, C. Jamet, G. Zibordi, T. Schroeder, and K. Stamnes, Atmospheric correction and aerosol retrieval over coastal waters using multilayer neural networks, Remote Sensing of the Environment, 199, 218-240, 2017.

Feng, H., Vandemark, D., Campbell, J. W., & Holben, B. N. (2008). Evaluation of MODIS ocean color products at a northeast United States coast site near the Martha's Vineyard Coastal Observatory. International of Remote Sensing, 29, 4479–4497.

Fischer and H. Grassl, "Radiative transfer in an atmosphere–ocean system: An azimuthally dependent matrixoperator approach." Appl. Opt. **23**, 1035–1039 (1984).

Frouin, R., B., Franz, A., Ibrahim, K., Knobelpiesse, Z., Ahmad, B., Cairns, J., Chowdhary, H.M., Dierssen, J., Tan, O., Dubovik, X., Huang, A.B., Davis, O., Kalashnikova, D.R., Thompson, L.A., Remer, E., Boss, O., Coddington, P.-Y., Deschamps, B.-C., Gao, L., Gross, O., Hasekamp, A., Omar, B., Pelletier, D., Ramon, F., Steinmetz and P.-W., Zhai (2019). Atmospheric correction of satellite ocaen-color imagery during the PACE era, Frontiers in Earth Sciences, 7, doi: 10.3380/feart.2019.00145.

Gordon, H.R. (1997). Atmospheric correction of ocean color imagery in the Earth Observing System era, Journal of Geophysical Research, 102, 17081-17106.

Gordon, H.R., and M., Wang (1994). Retrieval of water-leaving radiance and aerosol optical thickness over the ocean with SeaWiFS: a preliminary algorithm, Applied Optics, 443-452.

Hamre, B., S. Stamnes, K. Stamnes, and J.J. Stamnes, A versatile tool for radiative transfer simulations in the coupled atmosphere-ocean system: Introducing AccuRT, Ocean Optics XXII, Portland, ME, 2014.

Han, B., H., Loisel, V., Vantrepotte, X., Mériaux, P., Bryère, S., Ouillon, D., Dessailly, Q., Xing and J., Zhu (2016). Development of a semi-analytical algorithm for the retrieval of suspended particulate matter from remote sensing over clear to very turbid waters, Remote Sensing, 8, doi: 10.3390/rs8030211.

He, X., Y. Bai, D. Pan, J. Tang, and D. Wang, "Atmospheric correction of satellite ocean color imagery using the ultraviolet wavelength for highly turbid waters," Opt. Express 20(18), 20754–20770 (2012).

Holben, B., T.F., Eck, I., Slutsker, D., Tanré, J.P., Buis, A., Setzer, E., Vermote, J.A., Reagan, Y.J., Kaufman, T., Nakajima, F., Lavenu, I., Jankowiak and A., Smirnov (1998). AERONET - A federated instrument networks and data archive for aerosol characterization, Remote Sensing of Environment, 66, 1-16.

Hu, C., K.L., Carder and F.E., Muller-Karger (2000). Atmospheric correction of SeaWiFS imagery over turbid coastal waters: a practical method, Remote Sensing of Environment, 74, 195-206.

Ibrahim, A., B.A., Franz, Z., Ahmad and S.W., Bailey (2019). Multiband atmospheric correction algorithm for ocean color retrievals, Frontiers in Earth Science, 7, doi: 10.3389/feart.2019.00116.

IOCCG (2010). Atmospheric Correction for Remotely-Sensed Ocean-Colour Products. Wang, M. (ed.), Reports of the International Ocean-Colour Coordinating Group, No. 10, IOCCG, Dartmouth, Canada.

Jamet., C., S., Thiria, C., Moulin and M., Crepon (2004). Use of a neurovariational inversion for retrieving oceanic and atmospheric constituents from ocean color imagery: a feasibility study, Journal of Atmospheric and Oceanic Technology, 22, 460-475.

Keshava, N. (2004). Distance metrics and band selection in hyperspectral processing with applications to material identification and spectral libraries, IEEE Transactions on Geoscience and Remote Sensing, 42, 1552-1565.

Kruse, F., A., Lefkoff, J., Boardman, J., Heidebrecht, A., Shapiro, P., Barloon and A., Goetz (1994). The spectral image processing system -interactive visualization and analysis of imaging spectrometer data, Remote Sensing of Environment, 44, 145-163.

Kuchinke, C.P., H.R., Gordon, L.W., Harding, and K.J., Voss (2009). Spectral optimization for constituent retrieval in case 2 waters: II Implementation and performance, Remote Sensing of Environment, 13, 571-587.

Lavender, S.J., M.H., Penkerton, G.F., Moore, J., Aiken and D., Blondeau-Patissier (2005). Modification to the atmospheric correction of SeaWiFS ocean color images over turbid waters, Continental Shelf Research, 25, 539-555.

Mobley, C.D., J., Werdell, B., Franz, Z., Ahmad and S., Bailey (2016). Atmospheric correction for satellite ocean color radiometry - A tutorial and documentation of the algorithms used by the NASA Ocean Biology Processing Group, NASA report, 80 pages.

Moore, G.F., J., Aiken, and S.J., Lavender (1999). The atmospheric correction of water color and the quantitative retrieval of suspend particulate matter in case II waters: Application to MERIS, International Journal of Remote Sensing, 20, 1713-1733.

Moulin, C., H.R., Gordon, V.F., Banzon and R.H., Evans (2001a). Assessment of Saharan dust absorption in the visible from SeaWiFS imagery, Journal of Geophysical Research, 106, 18239-18249.

Moulin, C., H.R., Moulin, R.M., Chomko, V.F., Banzon and R.H., Evans (2001b). Atmospheric correction of ocean color imagery through thick layers of Saharan dust, Geophysical Research Letters, 28, 5-8.

Müller, D., J., Krasemann, R.J., Brewin, C., Brockmann, P.-Y., Deschamps, R., Doerffer, N., Fomferra, B.A., Franz, M.G., Grant, S.B., Groom, F. Mélin, T., Platt, P., Regner, S., Sathyendranath, F., Steinmetz and J., Swinton (2015). The Ocean Colour Climate Initiative: I. A methodology for assessing atmospheric correction processors based on in-situ measurements, Remote Sensing of Environnment, 162, 242-256.

Nobileau, D., and D., Antoine (2005). Detection a blue-absorbing aerosols using near infrared and visible (ocean color) remote sensing observations, Remote Sensing of Environment, 95, 368-387.

Oo, M., M., Vargas, A., Gilerson, B., Gross, F., Moshary and S., Ahmed (2008). Improving atmospheric correction for highly productive coastal waters using the shortwave infrared retrieval algorithm with water-leaving reflectance constraints at 412 nm, Applied Optics, 2008, 47, 3846-3859.

Park, Y.-J. & Ruddick, K. Model of remote-sensing reflectance including bidirectional effects for case 1 and case 2 waters. Appl. Opt., OSA, 2005, 44 , 1236-1249

Robinson, W.D., B.A., Franz, F.S., Patt, S.W., Bailey, and P.J., Werdell (2003). Masks and flags updates. In S. B. Hooker, & E. R. Firestone (Eds.), SeaWiFS Postlaunch Technical Report Series, Chap.6, NASA/TM-2003-206892. Greenbelt, Maryland, NASA Goddard Space Flight Center volume 22, 34–40.

Ruddick, K.G. and the COASTCOLOUR team (2010). DUE CoastColour Round Robin Protocol v1.2, 27 pages.

Sanwlani, N., P., Chauhan and R.R., Navalgung (2014). Atmospheric correction based on inherent optical properties of sea water at NIR wavelengths combined with an automated aerosol spectra determination (ASD) technique, International Journal of Remote Sensing, 35, 3631-3650.

Schroeder, T., I. Behnert, M. Schaale, J. Fischer, and R. Doerffer (2007). Atmospheric correction algorithm for MERIS above case-2 water, International Journal of Remote Sensing, 28, 1469-1486.

Schroeder, T., M. Schaale, and J. Fischer (2007). Retrieval of atmospheric and oceanic properties from MERIS measurements: A new Case-2 water processor for BEAM, International Journal of Remote Sensing, 28, 24, 5627-5632.

Shi, W., and M., Wang (2007). Detection of turbid waters and absorbing aerosols for the MODIS ocean color data processing, Remote Sensing of Environment, 110, 149-161.

Shi, C., and T., Nakajima (2018). Simultaneous determination of aerosol optical thickness and water-leaving radiance from multispectral measurements in coastal waters, Atmospheric Chemistry and Physics, 18, 3865-3884.

Siegel, D.A., M., Wang, S., Maritorena and W., Robinson (2000). Atmospheric correction of satellite ocean color imagery: the black pixel assumption, Applied Optics, 39, 3582-3591.

Singh, R.K., Shanmugam, P., 2014. A novel method for estimation of aerosol radiance and its extrapolation in the atmospheric correction of satellite data over optically complex oceanic waters. Remote Sens. Environ. 142, 188–206. https://doi.org/10.1016/j.rse.2013.12.001

Stamnes, K., W., Li, B., Yan, H., Eide, A., Barnard, W.S., Pegau and J.J., Stamnes (2003). Accurate and self-consistent ocean color algorithm: simultaneous retrieval of aerosol optical properties and chlorophyll concentrations, Applied Optics, 42, 939-951.

Steinmetz, F.; Deschamps, P.-Y. & Ramon, D. Atmospheric correction in presence of sun glint: application to MERIS. Optics Express, Optical Society of America, 2011, 19, 9783-9800

Stumpf, R.P., R.A., Arnone, R.W., Gould, P., Martinolich and V., Ransibrahmanakul (2003). Algorithm updates for the fourth SeaWiFS data reprocessing, Eds. S.B., Hooker, in SeaWiFS Postlaunche Technical Report Series, NASA Technical Memorandum 2003-206892, 51-59.

Thomas, G. E. and K. Stamnes, Radiative Transfer in the Atmosphere and Ocean, Cambridge University Press, 1999; second edition, 2002.

Van der Zande, D., Q., Vanhellemont, and K., Ruddick (2016). Validation of Landsat-8/OLI for ocean colour applications with AERONET-OC sites in Belgian coastal waters, Proceedings of the 2016 Ocean Optics Conference, Victoria, BC, Canada, 23-28 October 2016.

Wang, M. (2007). Remote sensing of the ocean contributions from ultraviolet to near-infrared using the shortwave infrared bands: simulations, Applied Optics, 46, 1535-1547.

Wang, M., and W., Shi (2005). Estimation of the ocean contribution at the MODIS near-infrared wavelengths along the east coast of the U.S.: Two case studies, Geophysical Research Letters, 32, doi: 13160.11029/12005GL022917.

Wang, M., and W., Shi (2007). The NIR-SWIR combined atmospheric correction approach for MODIS ocean color data processing, Optics Express, 15, 15722-15733.

Wang, M., and L. Jiang (2018). Atmospheric correction using the information from the short blue band, IEEE Transactions on Geoscience and Remote Sensing, 56, 6224-6237.

Wang, M., J., Tang, and W., Shi (2007). MODIS-derived ocean color products along the Chine east coastal region, Geophysical Research Letters, 34, doi: 06610.01029/02006GL028599.

Wei, J., Z.P., Lee and S., Shang (2016). A system to measure the data quality of spectral remote-sensing reflectance of aquatic environments, Journal of Geophysical Research, 121, 8189-8207, doi: 10.1002/2016JC012126.

Zibordi, G., B., Holben, F., Mélin, J.-F., Berthon, I., Slutsker, D., Giles, D., Vandemark, G., Feng, K., Rutledge, G., Schuster, A., Al Mandoos (2006). A network for standardized ocean color validation measurements, EOS Transaction AGU, 87, 293-304.

Zibordi, G., Berthon, J. -F., Mélin, F., D'Alimonte, D., & Kaitala, S. (2009a). Validation of satellite ocean color primary producs at optically complex coastal sites: Northern Adriatic Sea, Northern Baltic Proper and Gulf of Finland. Remote Sensing of Environment, 113, 2574–2591.

Zibordi, G., B., Holben, I., Slutsker, D., Giles, D., D'Alimonte, F., Mélin, J.-F., Berthon, D., Vandemark, H., Feng, G., Schuster, B.E., Fabbri, S., Kaitala and J., Sepala (2009b). Aeronet-oc: A network for the validation of ocean color primary products. Journal of the Atmospheric and Oceanic Technology, 26, 1634–1651.

Zibordi, G., F., Mélin, J.-F., Berthon and M., Talone (2015). In situ autonomous optical radiometry measurements for satellite ocean color validation in the Western Black Sea, Ocean Science, 11, 275-286.